Supporting Information

D'Este et al. 10.1073/pnas.1619553114

SI Materials and Methods

Primary Hippocampal Neuron Culture Preparation and Immunostaining. Cultures of hippocampal neurons were prepared from Wistar rats of mixed sex at postnatal day P0–P1. Cells were plated on coverslips coated with 100 μg/mL polyornithine (Sigma-Aldrich, cat. no. P3655) and 1 μg/mL laminin (BD Bioscience, cat. no. 354232). Neuronal cultures were maintained in Neurobasal medium (Gibco, cat. no. 21103049) supplemented with 2% B27 serum-free supplement (Gibco, cat. no. 17504044), 2 mM L-glutamine (Gibco, cat. no. 25030), and pen/strep (100 units per milliliter and 100 μg/mL, respectively; BiochromAG, cat. no. A2213). On the day after plating, 5 μM cytosine β-D-arabinofuranoside (Sigma-Aldrich, cat. no. C1768) was added to the cultures.

For immunostainings, cells were washed with PBS and fixed in 4% PFA in PBS (pH 7.4) for 20 min at room temperature, quenched with ammonium chloride and glycine (100 mM each) for 5 min, permeabilized with 0.1% Triton X-100 for another 5 min, and blocked in PBS supplemented with 1% BSA for 30 min. Both primary and secondary antibody and phalloidin incubations were performed in PBS for 1 h at room temperature or overnight at 4 °C. Samples were mounted in Mowiol supplemented with DABCO.

Molecular Lattices Simulation. As the molecular lattices are not expected to be complete, a simulation was performed to analyze the effect of missing molecules (see Fig. S2). A set of images with realistic values of resolution (~60 nm full width at half maximum), pixel size (30 nm), fluorescence intensity (Poissonian mean of 15 counts at peaks), and background (mean 5 counts per pixel) were generated, and the correlation analysis was performed for different lattice arrangements and filling factors.

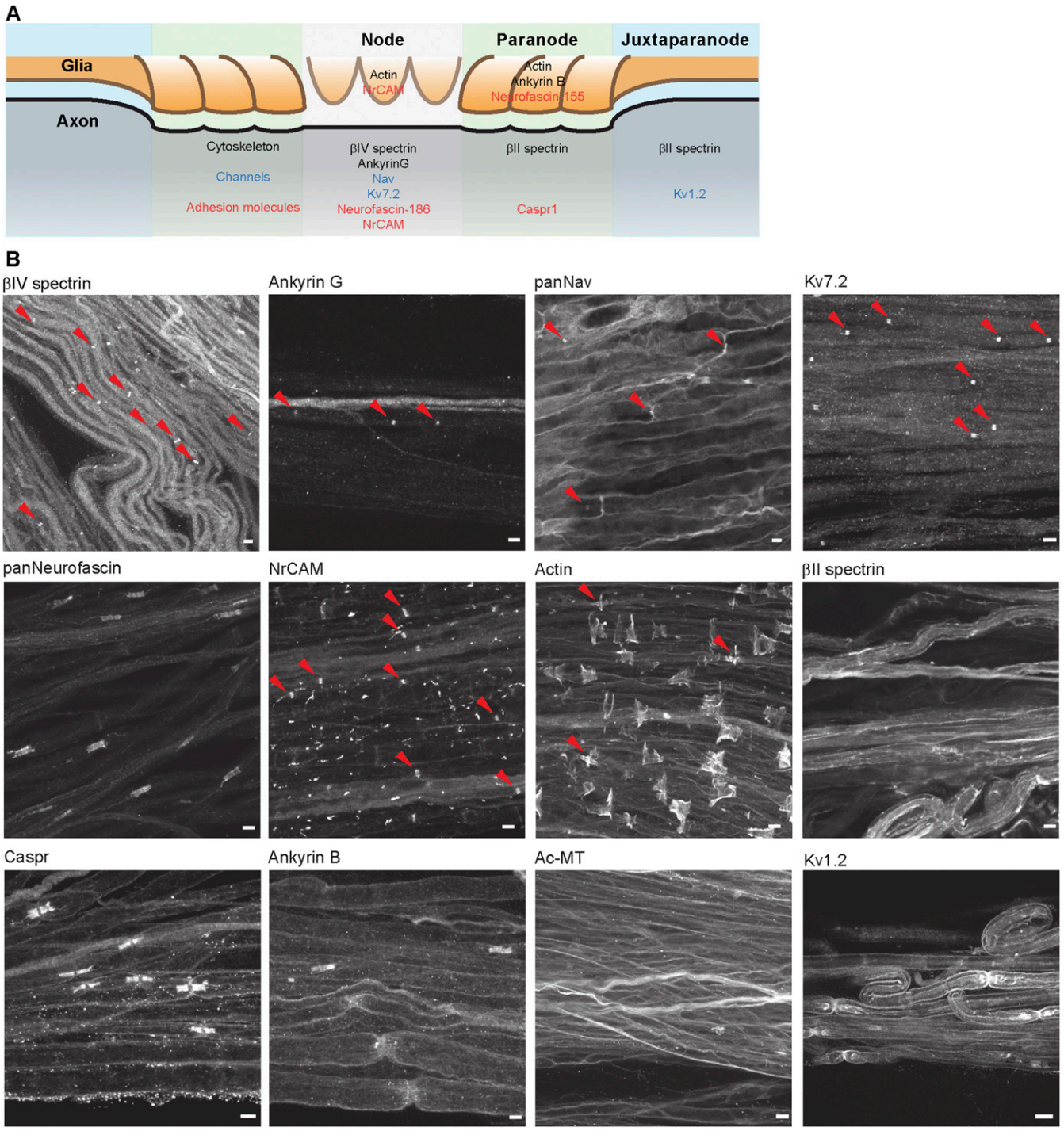

Fig. S1. Confocal images of the proteins analyzed in this study show uniform antibody labeling throughout the samples. (*A*) Schematic visualization of the structure of a node of Ranvier. The proteins analyzed in this study are listed in the region in which they are present and color-coded according to their function (black, cytoskeletal proteins; blue, channels; red, adhesion molecules). (*B*) Representative confocal images of the analyzed proteins. Red arrowheads point at nodal gaps. (Scale bars, 5 μm.)

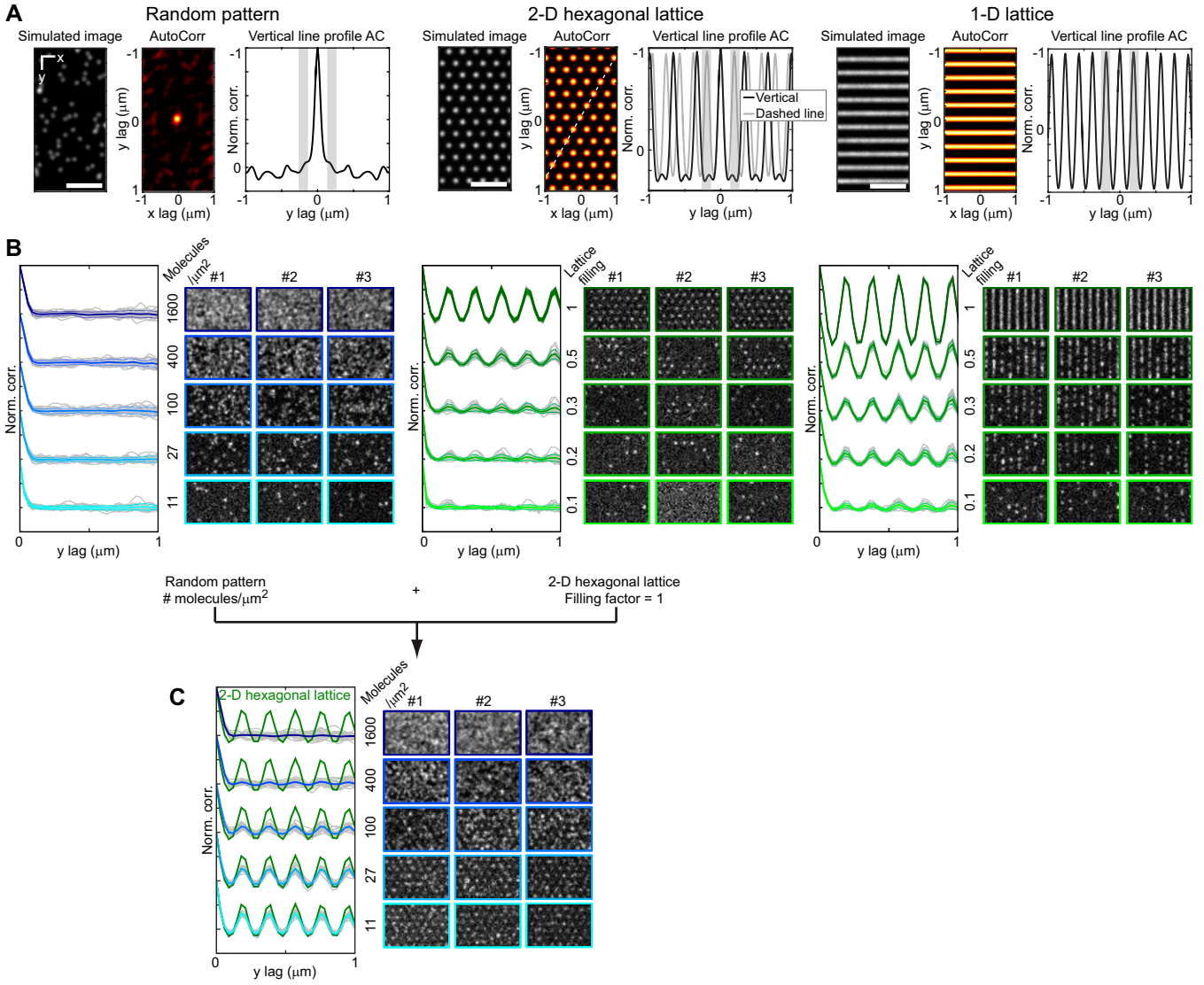

Fig. S2. Simulations of defined patterns and sensitivity of AC in the identification of periodic structures. (*A*) Background-free simulated images of a random pattern (27 molecules per square micrometer), of a 2D hexagonal lattice, and of a one-dimensional longitudinal lattice with 190-nm periodicity (simulated image, *Left*). Corresponding ACs (AutoCorr, *Middle*) and profile of intensities along a 1-pixel vertical line passing through the center of the AC (vertical line profile AC, *Right*) are shown. The gray bars are centered at ±0.2 μm *y* lag, where the peaks of periodicity are expected. No periodic peaks are visible in the random pattern, whereas both the 2D and one-dimensional lattices reveal a high periodicity and peak amplitude. In the case of the 2D hexagonal lattice, the vertical line profile has a ∼330-nm periodicity (black line), however the profile along a 30° tilted line (dashed line on the AutoCorr image) generates ∼190-nm peaks (gray line). Simulated images are 1 × 2 μm, and therefore, their size is comparable to the size of nodal gaps. (Scale bars, 500 nm.) (*B*) Simulation of the vertical line profile of the AC for different densities of molecules for the random pattern and different lattice filling factors for the other patterns. The lattice filling factor is the probability of having a lattice position occupied by a molecule. Because the AC is symmetrical, only half of the graph is depicted. For the one-dimensional lattice, molecules have been placed along a line every ∼40 nm. Indeed, in red blood cells, subcortical actin filaments are ∼40 nm long (28). For each parameter, the average line profile AC (thicker colored lines), the variance (thinner colored lines), and the profiles of each of the 50 simulations (gray lines) are shown. The AC analysis does not show any peak regardless of the density of molecules in the case of a random pattern. On the contrary, one-dimensional and 2D lattices exhibit periodic peaks already at low filling values (0.1 and 0.2, respectively), therefore proving the high sensitivity of AC. (*C*) Simulation of a mixed population of molecules. The 2D hexagonal lattice (filling factor = 1) was overlapped with different densities of randomly positioned molecules. For each parameter, the average line profile AC (thicker blue lines) with respect to the 2D hexagonal lattice (green lines) and the profiles of each of the 50 simulations (gray lines) are shown. The amplitude of peaks in the AC analysis is attenuated by the simultaneous presence of randomly positioned molecules and the effect increases with their concentration. A high concentration of random molecules overlaid to a perfect lattice completely hides the lattice, making it not detectable by the AC. Therefore, the presence of peaks in the AC is a robust measurement, as it can detect the presence of periodic structures almost regardless of the density of molecules and even in the presence of molecules that are not incorporated in the lattice. Simulated images on the right are 1 × 2 μm in size.

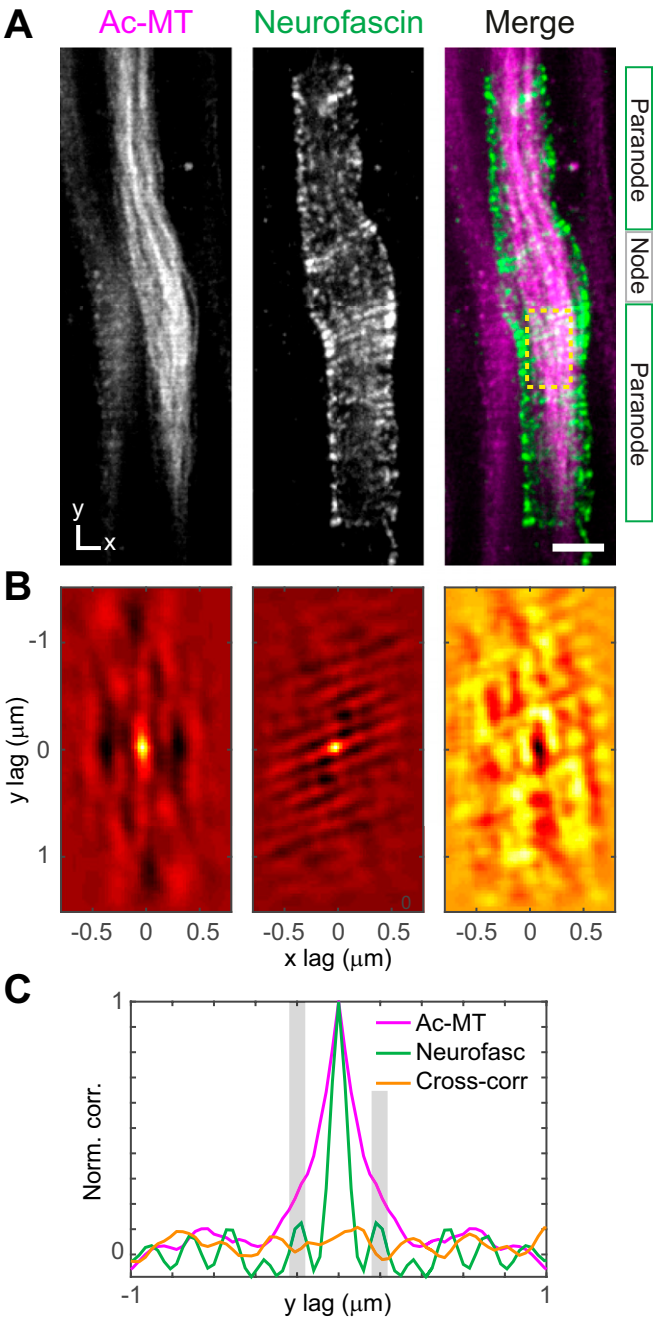

Fig. S3. Auto- and cross-correlation of linear structures do not exhibit periodic peaks. (*A*) Two-color STED images of a node and paranodes labeled with acetylated tubulin (*Left*) and neurofascin (*Middle*) and the overlay of the channels (*Right*). Microtubules form linear structures running along the axon. On the right, the regions of the node are indicated. (*B*) AC (for single-channel images) and cross-correlation (for the merged image) of the region indicated by the yellow dashed box in *A* (*y* axis along the axon). AC of microtubules does not show any periodic feature, whereas a one-dimensional order is present for neurofascin. (*C*) Vertical line profiles of intensities along the *y* axis of the panels shown in *B* show the absence of periodic features for microtubules, whereas neurofascin exhibits a periodic arrangement. Cross-correlation does not indicate the presence of any pattern in the relative positioning of the two proteins, therefore proving the specificity of the signal observed in the following experiments. Gray bars highlight the ±0.2 μm *y* lag. All image data were smoothed with a 1-pixel low-pass Gaussian filter. (All scale bars, 1 μm.)

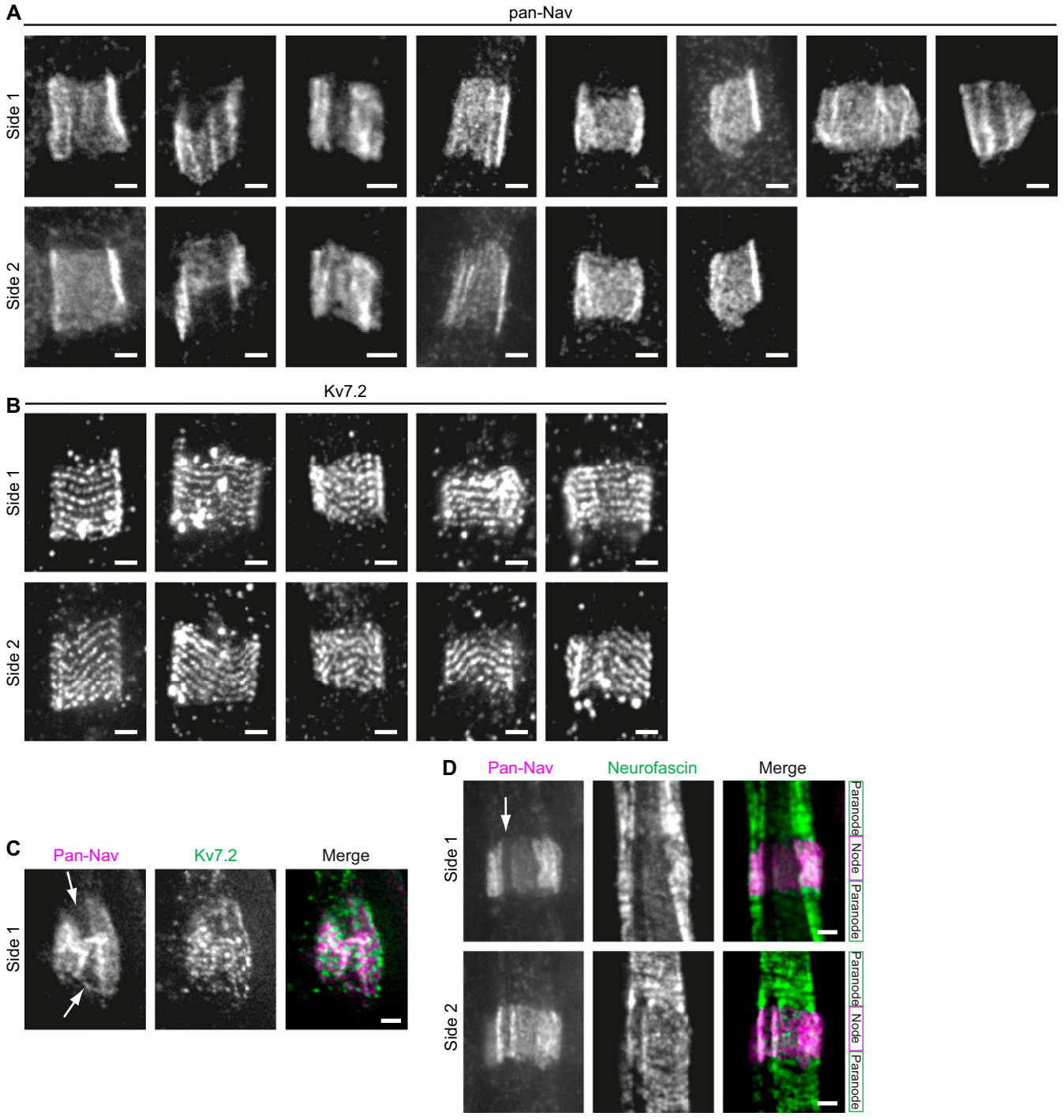

Fig. S4. Nanoscale organization of proteins at the nodal gap is often inhomogeneous and asymmetrical. (*A*) Examples of nodes stained with a pan-Na_v channel antibody. When possible, the opposite sides of the same node (side 1 and side 2) are shown. The staining often appears inhomogeneous and asymmetrical on the opposite side. (*B*) Examples of nodes stained with a K_v7.2 antibody directed against the N terminus. The opposite sides of the same node (side 1 and side 2) are shown. Different geometries in the organization of the nodes are visible on the opposite side of the nodes. The third node – side 1, as presented in Fig. S5*A*. (*C*) Costainings of Na_v channels (magenta) and K_v7.2 (N terminus, green) indicate that the grooves (arrows) are depleted from both proteins. (*D*) Costaining of Na_v channels (magenta) and neurofascin (green) shows a similar behavior of the two proteins and the lack of both species from the groove (arrow). On the right, the regions of the node are indicated. All image data were smoothed with a 1-pixel low-pass Gaussian filter and represent the overlay of several optical sections. (All scale bars, 500 nm.)

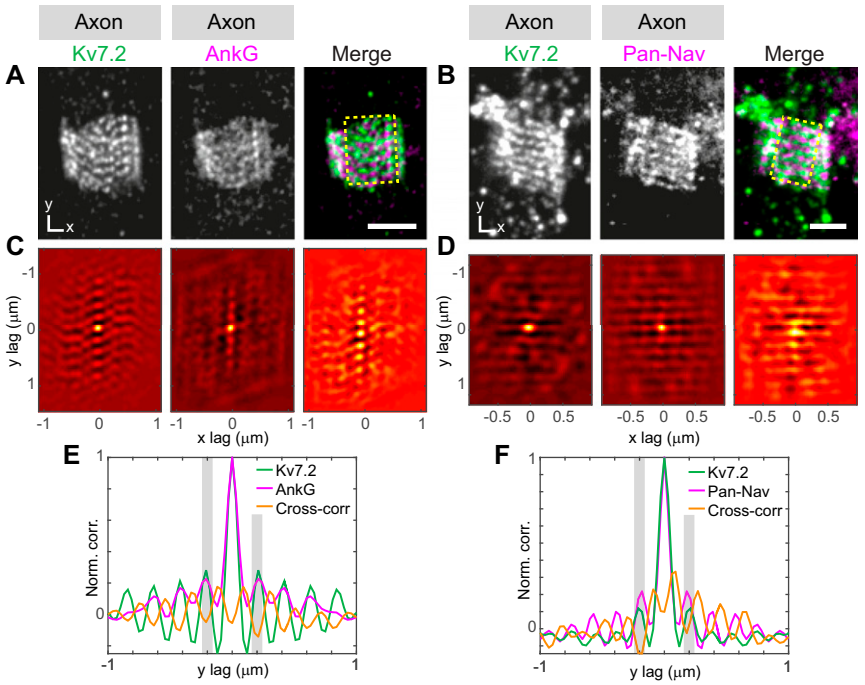

Fig. S5. $K_v7.2$ channels intercalate with both ankyrin G and Na_v channels. Two-color STED images of nodes labeled for (*A*) $K_v7.2$ (N terminus, *Left*) and ankyrin G (monoclonal antibody, *Middle*) or (*B*) $K_v7.2$ (C terminus, *Left*) and pan-Na_v (*Middle*). Single-color images and overlays are shown. For both combinations of proteins, an alternating pattern is observed. (*C* and *D*) AC (for single-channel images) and cross-correlation (CC, for the merged image) of the regions indicated by the yellow dashed boxes in *A* and *B*. The *y* axis is aligned with the axon. A longitudinal periodicity can be observed for all AC and CC. (*E* and *F*) Vertical line profile of intensities along the panels shown in *C* and *D*, respectively. The gray bars highlight the ±0.2 μm *y* lag. All proteins show peaks at the same position, and cross-correlation indicates a phase shift of the proteins. The node in *A* is also presented in Fig. S4*B* (third image). All image data were smoothed with a 1-pixel low-pass Gaussian filter and represent the overlay of several optical sections. (All scale bars, 1 μm.)

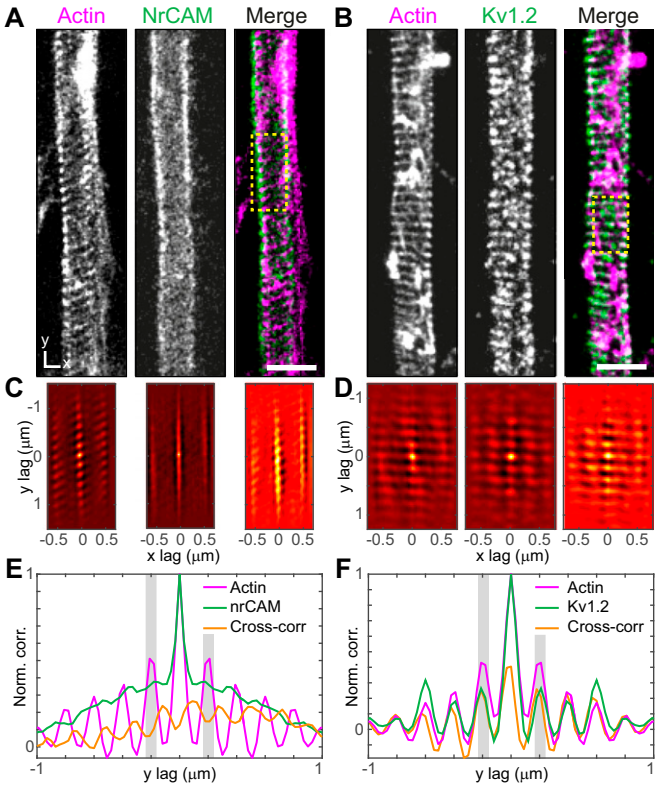

Fig. S6. Periodic organization of NrCAM and $K_v1.2$ along the AIS of hippocampal neurons. STED image of AIS labeled with phalloidin to stain F-actin (*Left*), (*A*) NrCAM (31 d in vitro) or (*B*) $K_v1.2$ (29 d in vitro) (*Middle*), and the overlay of the two channels (*Right*). (*C* and *D*) AC (for single channel images) and cross-correlation (for the merged image) of the regions indicated by the yellow dashed boxes in *A* and *B* (*y* axis along the axon) show a strong longitudinal pattern. (*E* and *F*) Vertical line profiles of intensities along the *y* axis of the panels shown in *C* and *D* show a weak NrCAM periodicity that is out-of-phase with actin, whereas $K_v1.2$ has a pronounced, in-phase organization. Gray bars highlight the ±0.2 μm *y* lag. All image data were smoothed with a 1-pixel low-pass Gaussian filter. (All scale bars, 1 μm.)

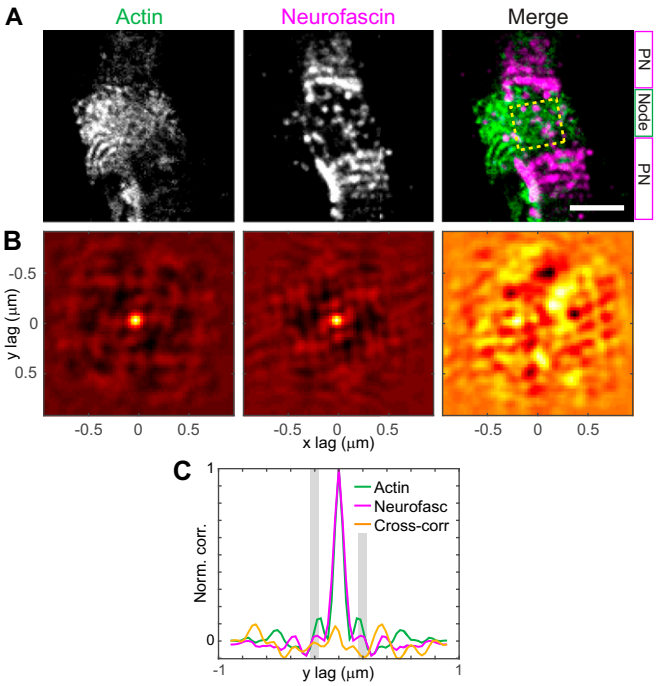

Fig. S7. Correlation between actin and neurofascin at the nodes of Ranvier. (*A*) STED image of a node stained with phalloidin to mark F-actin (*Left*), neurofascin (*Middle*), and the overlay of the two channels (*Right*). On the right, the regions of the node are indicated. PN, paranode. Same node as shown in Fig. 3. (*B*) AC (for single-channel images) and cross-correlation (for the merged image) of the region indicated by the yellow dashed box in *A* do not show a predominantly longitudinal organization. (*C*) Vertical line profile of intensities along the panels shown in *B* reveals periodic peaks at ∼190 nm (gray bars centered at ±200 μm *y* lag) and an out-of-phase cross-correlation. All image data were smoothed with a 1-pixel low-pass Gaussian filter and represent the overlay of several optical sections. (Scale bar, 1 μm.)

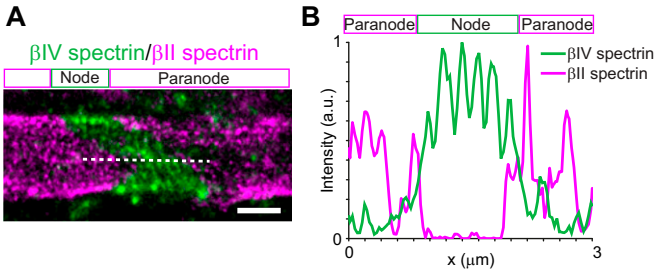

Fig. S8. The spectrin scaffold is uninterrupted at the transition between node and paranodes. (*A*) STED image of a sciatic nerve in which both betaII spectrin (paranodes) and betaIV spectrin (node) have been labeled. (*B*) Profile of intensities for the two channels along the dashed line (5-pixel width) in *A* shows the continuity of the spectrin lattice at the transition between paranodes and node. Image data were smoothed with a 1-pixel low-pass Gaussian filter and represent the overlay of several optical sections. (Scale bar, 1 μm.)

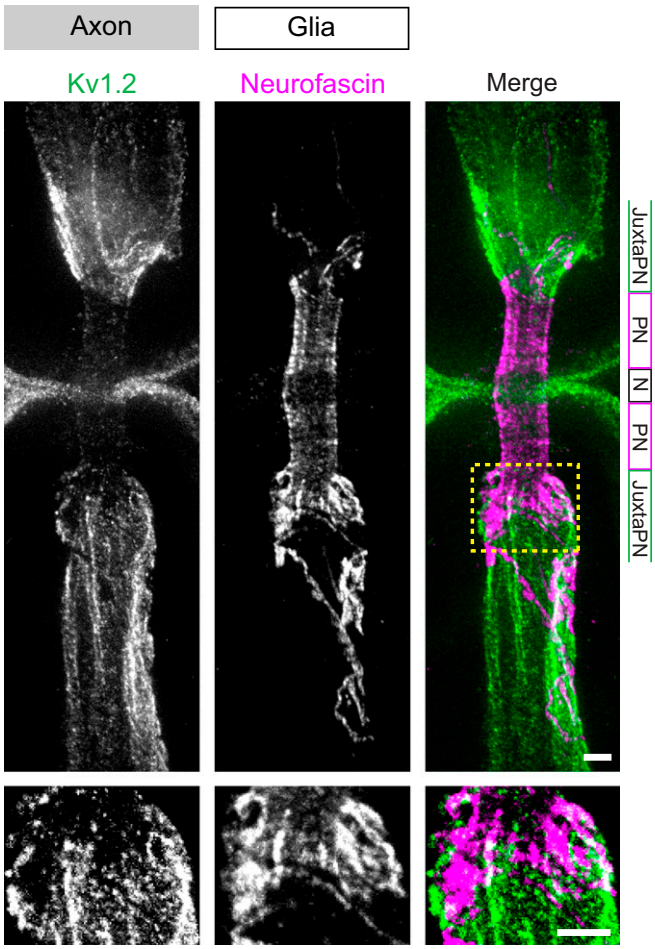

Fig. S9. $K_v1.2$ channels do not show a periodic organization at juxtaparanodes and are complementary to neurofascin. STED image of a nerve stained for $K_v1.2$ (*Left*), neurofascin (*Middle*), and the overlay of the two channels (*Right*). On the right, the regions of the node are indicated. JuxtaPN, juxtaparanodes; N, node; PN, paranode. (*Bottom*) Close-up of the region indicated by the yellow dashed box reveals almost no overlay of the two proteins. All image data were smoothed with a 1-pixel low-pass Gaussian filter and represent the overlay of several optical sections. (Scale bar, 1 μm.)